Available online at www.sciencedirect.com
ScienceDirect
Control Engineering Practice 15 (2007) 825–837
CONTROL ENGINEERING PRACTICE
www.elsevier.com/locate/conengprac

A controller enabling precise positioning and sway reduction in bridge and gantry cranes

Khalid L. Sorensen, William Singhose*, Stephen Dickerson

The George W. Woodruff School of Mechanical Engineering, Georgia Institute of Technology, 813 Ferst Dr., MARC 257, Atlanta, GA 30332-0405, USA

Received 28 September 2005; accepted 30 March 2006
Available online 5 June 2006

Abstract

Precise manipulation of payloads is difficult with cranes. Oscillation can be induced into the lightly damped system by motion of the bridge or trolley, or from environmental disturbances. To address both sources of oscillation, a combined feedback and input shaping controller is developed. The controller is comprised of three distinct modules. A feedback module detects and compensates for positioning error; a second feedback module detects and rejects disturbances; input shaping is used in a third module to mitigate motion-induced oscillation. An accurate model of vector drive and AC induction motors, typical to large cranes, was used jointly with a deconvolution analysis technique to incorporate the nonlinear dynamics of crane actuators into the control design. The controller is implemented on a 10-ton bridge crane at the Georgia Institute of Technology. The controller achieves good positioning accuracy and significant sway reduction.
© 2006 Elsevier Ltd. All rights reserved.

Keywords: Input shaping; Command shaping; Crane control; Oscillation control; Anti-sway; Bridge crane; Gantry crane

1. Introduction

Bridge and gantry cranes occupy a crucial role within industry. They are used throughout the world in thousands of shipping yards, construction sites, steel mills, warehouses, nuclear power and waste storage facilities, and other industrial complexes. The timeliness and effectiveness of this manipulation system are important contributors to industrial productivity. For this reason, improving the operational effectiveness of cranes can be extremely valuable.

These structures, like the one shown in Fig. 1, are highly flexible in nature. External disturbances, such as wind or motion of the overhead support unit (e.g. the bridge or trolley), can cause the payload to oscillate. In many applications these oscillations have adverse consequences. Swinging of the payload or hook makes precision positioning time consuming and inefficient for a human operator; furthermore, when the payload or surrounding obstacles are of a hazardous or fragile nature, the oscillations may present a safety risk (Khalid, Singhose, Huey, & Lawrence, 2004).

The broad usage of bridge and gantry cranes, coupled with the need to control unwanted oscillations, has motivated a large amount of research pertaining to the control of these structures. Engineers have sought to improve the ease-of-use, increase operational efficiency, and mitigate safety concerns by addressing three primary aspects of crane systems: (1) motion-induced oscillation; (2) disturbance-induced oscillation; and (3) positioning capability.

Singer et al. reduced motion-induced oscillations of a 15-ton bridge crane by using robust input shaping techniques (Singer, Singhose, & Kriikku, 1997). Fang et al. proposed to control final trolley position and motion-induced oscillation through proportional-derivative (PD) control in which the coupling between the cable angle and the motion of the trolley was artificially increased (Fang, Dixon, Dawson, & Zergeroglu, 2001). Piazzi proposed a dynamic-inversion-based control for reducing transient and residual motion-induced oscillation (Piazzi & Visioli,

*Corresponding author. Fax: +1 404 894 9342.
E-mail address: Singhose@gatech.edu (W. Singhose).

0967-0661/$ - see front matter © 2006 Elsevier Ltd. All rights reserved.
doi:10.1016/j.conengprac.2006.03.005

LIST OF FIGURES

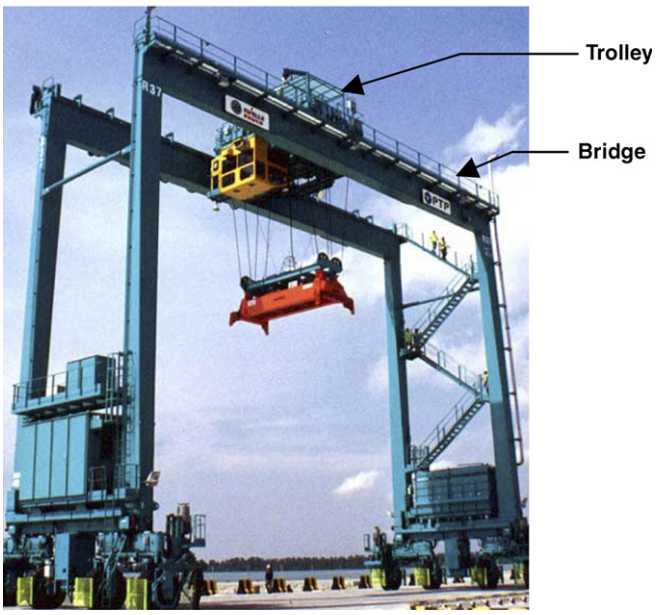

Fig. 1. Picture of a gantry crane at a shipping dock (courtesy of Favelle Favco Cranes).

2002). Kim implemented a pole-placement strategy on a real container crane to control motion and disturbance-induced oscillation, as well as final positioning (Kim, Hong, & Sul, 2004). Moustafa developed nonlinear control laws for payload trajectory tracking based on a Lyapunov stability analysis (Moustafa, 2001). O'Connor developed a control strategy based on mechanical wave concepts that involves learning unknown dynamics through an initial trolley motion (O'Connor, 2003). Finally, Fliess used a generalized state variable model suggested in (Fliess, 1989), and then proposed a linearizing feedback control law (Fliess, Levine, & Rouchon, 1991). The position of the trolley and length of the payload cable were the controlled variables, and their respective reference trajectories were limited to a class of fourth-order polynomials to insure minimal payload sway. The control did not attempt to eliminate disturbance-induced oscillations.

The control schemes developed in the literature may be broadly grouped into three categories: time-optimal control, command shaping, and feedback control. The implementation of these various control methods presents several challenges. A common difficulty is the behavior of drives and motors that actuate crane motion. Nonlinear behavior of these elements have been difficult to evaluate with traditional analysis techniques, and are, therefore, often neglected in controller designs.

A drawback related to time-optimal control is its inability to be implemented in real-time, owing to the necessity of precomputation of system trajectories. There is no known implementation of a time-optimal control scheme used with a commercial crane (Gustafsson & Heidenback, 2002).

Command shaping is a reference signal modification technique that is implementable in real time (Singer & Seering, 1990). However, command shaping does not have the closed-loop mechanisms of feedback control, and must, therefore, be used in conjunction with a feedback control if it is to be used for disturbance rejection.

Feedback control is the most common strategy used in research efforts to mitigate positioning and cable sway errors. This type of control is aptly suited for positioning a bridge or trolley. However, when a feedback controller must minimize cable sway, the control task becomes much more problematic. Accurate sensing of the payload must be implemented, which is often costly or difficult. These difficulties are discussed in detail for fully automatic commercial cranes in use at the Pasir Panjang terminal in Singapore (Gustafsson & Heidenback, 2002). Furthermore, feedback control schemes are somewhat slow because they are inherently *reactive*. For example, when feedback is utilized to control cable sway, cable sway must be present in the system before the control will attempt to eliminate the undesired oscillations.

One of the most useful techniques used for negating a system's flexible modes is input shaping. Input shaping does not require the feedback mechanisms of closed-loop controllers. Instead, the control reduces oscillations in an *anticipatory* manner, as opposed to the reactive manner of feedback. Oscillation suppression is accomplished with a *reference* signal that anticipates the error before it occurs, rather than with a *correcting* signal that attempts to restore deviations back to a reference signal. In the context of crane control, this means that sensing cable sway is not necessary. As a result, input shaping is easier to implement than feedback schemes. In many instances, input shaping techniques are also amenable to hard nonlinearities present in actuating drives and motors. Input shaping techniques have proven effective at significantly reducing motion-induced cable sway during crane motion (Kenison & Singhose, 1999; Lewis, Parker, Driessen, & Robinett, 1998; Singer et al., 1997; Singhose, Porter, Kenison, & Kriikku, 2000). Cranes utilizing the input shaping control also exhibited a significant improvement in efficiency and safety (Khalid et al., 2004).

The controller developed in this paper has been designed with positioning and oscillation suppression properties by merging feedback control with input shaping. The control is comprised of distinct modules that have been combined into a unified control architecture. Each module is designed to control one aspect of the crane's performance. A feedback control module is used to position the payload at a desired location, while a different feedback module rejects disturbances. Input shaping is used in a third module to minimize motion-induced oscillation.

This strategy of allocating individual control tasks to individual controllers is similar to the approach used by Sorensen, Singhose, and Dickerson (2005). The strategy helps mitigate design and implementation difficulties discussed previously by utilizing the strengths of the

different control modules for tasks they are most suited for, feedback for positioning and disturbance rejection, and input shaping for reducing motion-induced oscillation in the presence of hard nonlinearities. The performance of the control is evaluated experimentally on a 10-ton bridge crane located in the Manufacturing Research Center (MARC) at the Georgia Institute of Technology (Georgia Tech).

The following section provides a synopsis of crane system dynamics that incorporates the effects of nonlinear drives and motors. Section 3 presents a brief overview of the overall control system followed by a more detailed description of the individual modules comprising the controller. The stability of the two closed-loop modules is also discussed. Section 4 explains how the distinct modules are combined into a single control architecture, and examines the stability of the combined architecture. Section 5 contains concluding remarks. Experimental data are used throughout the paper to demonstrate key aspects of the control system.

2. Crane dynamics

The 10-ton MARC crane used to test the control described here is shown in Fig. 2. Planer motion of this crane can be simply modeled as a pendulum suspended from a moving support unit, as shown in Fig. 3. The mass of the overhead support unit and mass of the payload are labeled as m_t and m_p, respectively; acceleration due to gravity is represented as g; a viscous damping force, which acts on the payload, can be described by the damping coefficient b; and the length of the suspension cable is labeled as L. The trolley position, x, will be considered as the controlled variable. An obvious benefit to such a choice for the system input is that a model of crane motors and industrial drives is unnecessary at this juncture. Later these systems will be considered when determining the response

Fig. 2. Bridge crane in the Manufacturing Research Center.

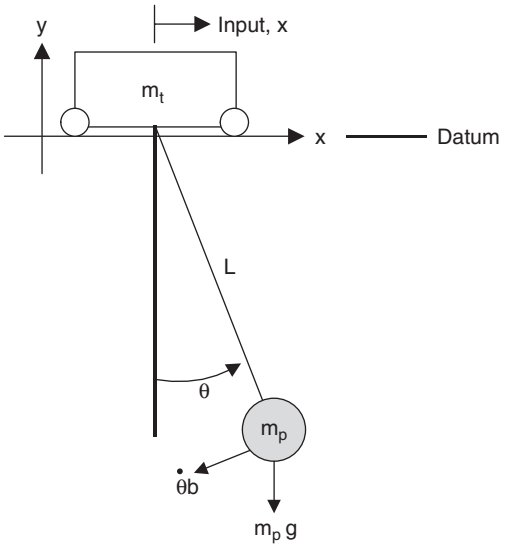

Fig. 3. Multi-body model of the crane along one axis.

of the system to reference signals. A similar modeling formulation was used in Fliess et al. (1991).

With the crane modeled in this manner, the system is reduced to one degree of freedom with the cable angle, θ, used as the independent coordinate.

The differential equation of motion is

$$\ddot{\theta} + \left(\frac{b}{Lm_p}\right)\dot{\theta} + \left(\frac{g}{L}\right)\sin\theta = \left(\frac{-\cos\theta}{L}\right)\ddot{x}. \tag{1}$$

The limited cable sway of crane systems allows one to assume a small angle approximation, reducing (1) to:

$$\ddot{\theta} + \left(\frac{b}{Lm_p}\right)\dot{\theta} + \left(\frac{g}{L}\right)\theta = \left(\frac{-1}{L}\right)\ddot{x}. \tag{2}$$

Recognizing that (2) represents a second-order damped oscillatory system, one may write

$$\left(\frac{b}{Lm_p}\right) = 2\zeta\omega_n, \tag{3}$$

$$\left(\frac{g}{L}\right) = \omega_n^2, \tag{4}$$

and

$$\left(\frac{-1}{L}\right) = -\frac{\omega_n^2}{g}. \tag{5}$$

To obtain a system representation relating the velocity of the overhead support unit to the angle of the cable one may substitute the time derivative of the support unit position, $\dot{v}_t$, for $\ddot{x}$. Assuming zero initial conditions, and using the relations in (3) through (5), one obtains the following transfer function relating the cable angle to the velocity of the support unit:

$$\frac{\Theta(s)}{V_t(s)} = \frac{(-\omega_n^2/g)s}{s^2 + 2\zeta\omega_n s + \omega_n^2}. \tag{6}$$

This relationship is represented as a block diagram in Fig. 4, where the block labeled as "Payload" represents the

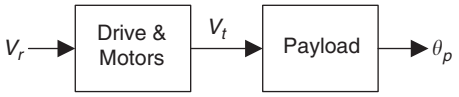

Fig. 4. Input velocity–output angle relationship for a crane.

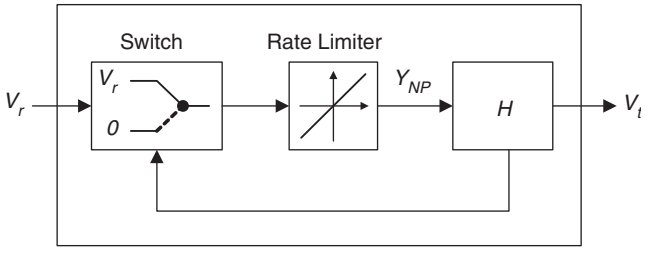

Fig. 5. Model of AC induction motors and vector drives.

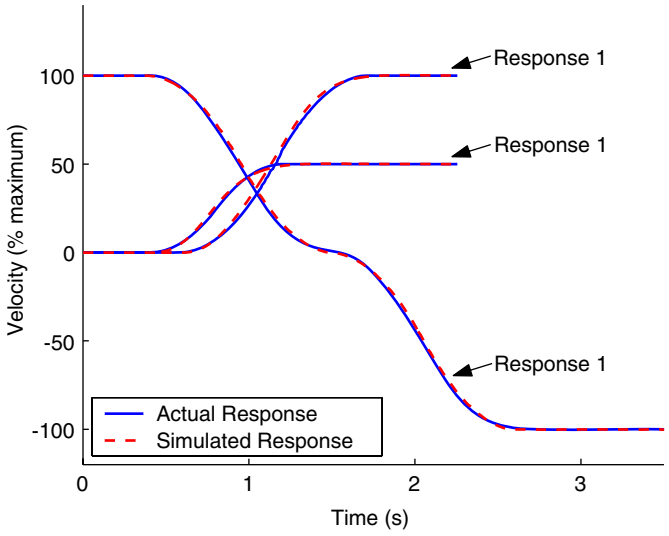

Fig. 6. Comparison of actual and simulated responses to several velocity commands.

transfer function expressed in (6). The velocity of the overhead support unit, V_t, causes the payload plant to respond with cable angle θ_p. Also illustrated in Fig. 4 is the relationship between the support unit velocity, V_t, and the desired reference velocity, V_r. The actual velocity of the support unit is the response of the plant labeled "Drive & Motors" to the reference velocity. This plant is a composite representation of the actuation elements and crane mass. These elements are comprised of the bridge and trolley masses, motors, and drives.

An accurate model of industrial AC induction motors, vector drives, and support unit mass, typical for large cranes, was derived in Sorensen (2005). This model is represented in the block diagram of Fig. 5.

The model relates the velocity response of drives and motors to a desired reference velocity. Three elements comprise the model: a switch, a rate limiter, and a linear, second-order, heavily damped plant, H. The switching element ordinarily passes the original reference signal, V_r, to the rate-limiting block. However, when transitional velocity commands are issued to the crane, the switch temporarily sends a signal of zero. Transitional velocity commands are those commands that change the direction of travel of the crane (forward to reverse or vise versa). This type of behavior depends on V_r and V_t, and can be described with the following switching rules:

$$\textit{Switch output} = \begin{cases} V_r, & \text{Sign}(V_r) = \text{Sign}(V_t), \\ V_r, & |V_t| \leqslant X\%, \\ 0, & \text{otherwise.} \end{cases} \quad (7)$$

This model may be used to represent the response of many industrial vector drive and AC induction motor combinations by proper selection of four parameters associated with the model: the slew rate parameter of the rate limiter, S; the switch percent of the switch element, $X\%$; the natural frequency of H; and the damping ratio of H. For the MARC crane, these parameters were estimated to be 160%/s, 0.9%, 6.98 rad/s, and 0.86, respectively.

The response of the model closely follows the actual response of the MARC crane. This can be seen in Fig. 6, where the response of the model and the response of the actual support unit to several velocity commands have been overlaid.

3. Combined input shaping and feedback control

The crane described in Section 2 is comprised of a linear payload plant and a nonlinear drive/motors plant. The control system described here generates reference velocity commands that, when issued to the nonlinear drive and motors, achieve three desirable results in the payload: (1) precise positioning; (2) motion-induced oscillation suppression; and (3) disturbance rejection. A block diagram of the overall control system is shown in Fig. 7.

The means by which the combined control accomplishes the three objectives is easily understood by separately considering the individual modules comprising the controller. The following subsections provide a description of each of the three modules. The stability of the closed-loop modules is also discussed.

3.1. Input shaping module

A successful approach to suppressing oscillation in linear plants is to generate a reference command that drives a system to cancel out its own oscillation. One such technique, input shaping, is implemented by convolving a sequence of impulses, known as an input shaper, with a reference signal (this process is illustrated in Fig. 8). The shaped command is then used to drive the linear system.

The amplitudes and time locations of the impulses comprising the input shaper are determined by solving a set of constraint equations that attempt to limit the unwanted system dynamics. All that is needed to solve the equations is an estimate of the system natural frequency and damping

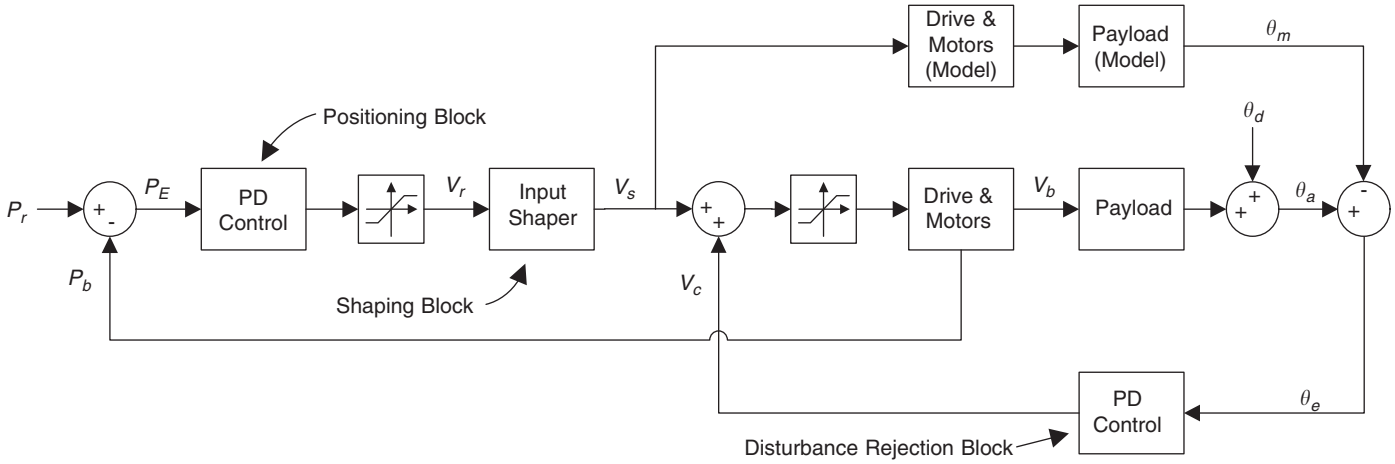

Fig. 7. Combined input shaping, positioning, and disturbance rejection controller.

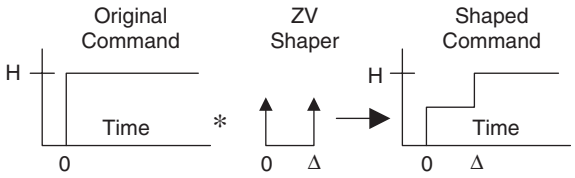

Fig. 8. The input shaping process.

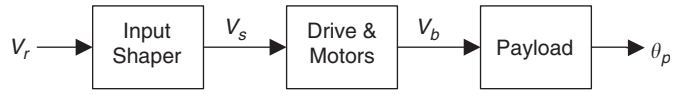

Fig. 9. Input shaping module.

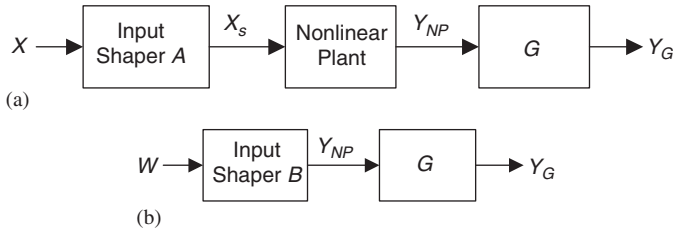

Fig. 10. Nonlinear and equivalent linear block diagrams: (a) generalized input shaping module and (b) equivalent input shaping module.

ratio. If the amount of residual oscillation produced by the sequence of impulses is set equal to zero, then a shaper satisfying the constraint equations is called a Zero Vibration (ZV) shaper (Singer & Seering, 1990; Smith, 1957). The ZV shaper shown in Fig. 8 has two impulses that change the original step command into a staircase shaped command. The rise time of the modified command is increased by the duration of the shaper, Δ.

Implementing input shaping on a physical system, such as the MARC crane, is accomplished in the manner shown in Fig. 9. The shaped commands are first sent to the drive and motors, then the response of the drive and motors actuate the payload.

Given this configuration, one must determine what influence the nonlinear drive and motors have on the ability of the shaped commands to eliminate oscillations from the payload. If the drive and motors can be represented as a linear transfer function, then there is no detrimental effect on the oscillation suppression of the input shaper; this is due to the commutability of the input shaper and linear plant. However, the model contains a nonlinear rate limiter, as well as a nonlinear switch; therefore the possibility of representation by a transfer function is precluded.

To understand the effects of the nonlinear drive and motors plant, consider the block diagram of a system shown in Fig. 10a where an arbitrary reference signal, X, is modified by input shaper A to produce a shaped command, X_s. Assume that the reference signal eventually obtains a steady-state value. Also assume that the input shaper is designed to cancel the oscillations of a linear plant, G. If X_s is used as an input to a nonlinear plant, such as the drive and motors model, then the response of the nonlinear plant may be represented as Y_{NP}.

The same nonlinear response, Y_{NP}, could be obtained by an alternate process where some baseline command, W, is modified by input shaper B (not necessarily consisting of an impulse sequence suitable for eliminating oscillations in G), reducing the system to that of Fig. 10b. This is an equivalent system that contains no nonlinear elements. Fig. 11 demonstrates this process when X is a step input, and the nonlinear plant consists of a rate limiter with slew rate parameter, S. Notice that an identical response, Y_{NP}, is generated by command W and ZV shaper B.

The process of resolving an arbitrary signal into a baseline command and an input shaper is called deconvolving. If it can be shown that the input shaper resulting from the deconvolution (shaper B) consists of an impulse sequence suitable for eliminating oscillations in G, and that the baseline command, W, obtains some steady-state value, then the nonlinear elements of the original system will have no detrimental effects on the oscillation suppression properties of the shaped signal, X_s. This is because the original system behaves as if the signal Y_{NP} was created by properly shaping a command for G. If both of these

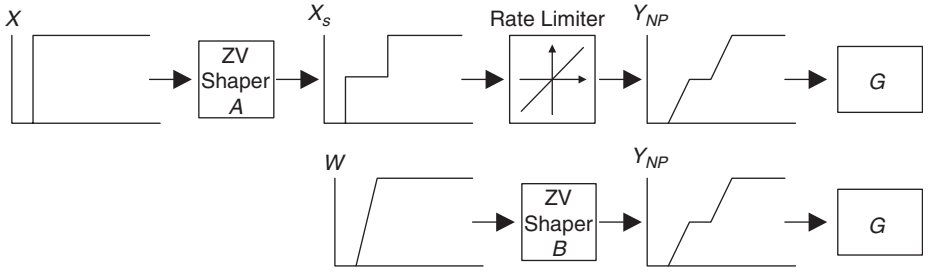

Fig. 11. Generating Y_{NP} from W and shaper B.

Table 1
Acceptable slew rates for a rate limiter following an input shaping module

Module Config-uration:	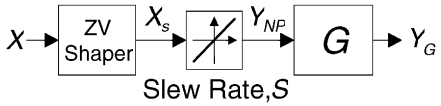
Acceptable R_{ZV} Values:	$1 \le R_{ZV} < \infty$, or $R_{ZV} = \frac{1}{n}$, $n = 1, 2, 3, \ldots$ $R_{ZV} = \frac{\Delta_{ZV}}{50\%} S$, $\Delta_{ZV} = Shaper \quad Duration$

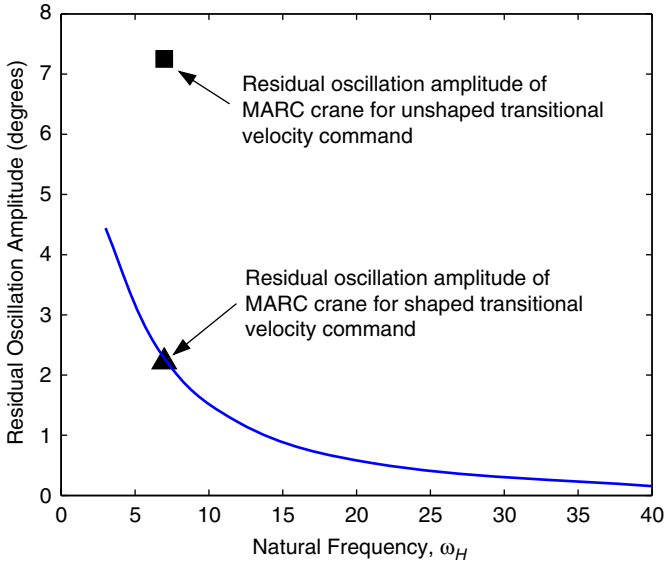

Fig. 12. Effects of the switching element on residual oscillation amplitude.

conditions cannot be met, then the nonlinear elements of the original system can diminish the oscillation reducing properties of the original input shaper.

To evaluate the detrimental effects of a rate limiter on a shaped command for *any* command X, and *any* slew rate parameter, S, one may perform an exhaustive deconvolution analysis for every combination of X and S. Of course this is not practical. Instead, one may quickly evaluate rate limiter effects through the use of a non-dimensional ratio R_{ZV}. This ratio relates how rapidly a rate limiter alters a reference signal to how rapidly a ZV input shaper alters a reference signal. It is defined as $R_{ZV} = (\Delta_{ZV}/50\%)S$, where Δ_{ZV} is the shaper duration. A rate limiting element has no detrimental effect on a ZV input shaper, regardless of the command X or parameter S, for the following range of R_{ZV}: $1 \leqslant R_{ZV} \leqslant \infty$, or $R_{ZV} = 1/n$, $n = 1, 2, 3, \ldots$. The R_{ZV} value for the MARC crane is well within acceptable limits. These results are summarized in Table 1.

The deconvolution analysis technique was also used to analyze the effects of the switching element on the ZV shaper (recall that the switching element affects motor response only when transitional velocity commands are issued to the crane). It was found that detrimental effects do exist, and that the severity of these effects varies approximately as the inverse of the natural frequency of H. Even so, given the value of H for the MARC crane, the induced oscillation caused by the switch element is still significantly lower than if shaping were not used. This is clearly demonstrated in Fig. 12. The solid line in this figure was obtained through simulations; it shows how the residual oscillation amplitude when input shaping is used varies with ω_H, the natural frequency of H. The triangle and square markers are the experimental oscillation amplitudes with and without shaping, respectively; their placement on the graph corresponds to the value of ω_H for the MARC crane.

In light of the foregoing results, one is assured that the input shaping module of Fig. 9 significantly reduces motion-induced oscillations in the payload, even in the presence of nonlinearities of the drive and motors plant.

The beneficial effects of input shaping were verified by having numerous operators drive the crane through a cluttered work environment both with and without input shaping (Khalid et al., 2004). While the crane was in motion, a downward looking video recorder captured the payload motion. Fig. 13 compares the responses from a typical trial. During unshaped motion the hook oscillated when the crane was commanded to move and after it was commanded to stop, in addition, the payload collided twice

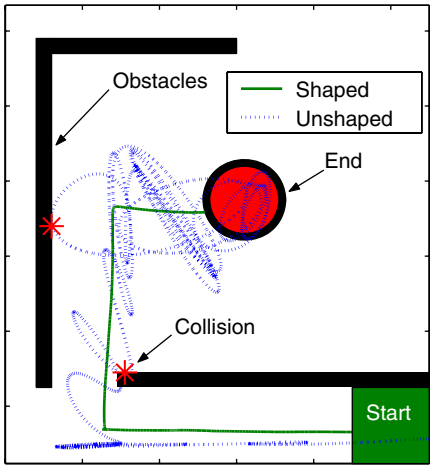

Fig. 13. Shaped and unshaped payload motion in a cluttered work environment.

with surrounding obstacles. In contrast, the shaped trajectory shows that the motion-induced oscillations were eliminated and no collisions occurred.

3.2. Positioning module

Consider again the transfer function in (6) that relates the cable angle to the velocity of the overhead support unit. A state space representation of this plant follows directly from the coefficients of the transfer function:

$$\dot{\boldsymbol{q}} = \mathrm{A}\boldsymbol{q} + \boldsymbol{b}v_t(t), \quad \theta(t) = \boldsymbol{cq}, \tag{8}$$

where

$$A = \begin{bmatrix} 0 & 1 \\ -\omega_n^2 & -2\zeta\omega_n \end{bmatrix}, \quad \boldsymbol{b} = \begin{bmatrix} 0 \\ 1 \end{bmatrix}, \text{ and } \boldsymbol{c} = \begin{bmatrix} 0 & \dfrac{-\omega_n^2}{g} \end{bmatrix}. \tag{9}$$

Given the relationship between q_2 and θ established in (8), one may recognize that the state q_2 is equal to $-\theta L$, the relative horizontal displacement between the trolley and the payload.

Computing the eigenvalues of A, we have

$$\lambda = -\zeta\omega_n \pm \omega_d \mathrm{i}. \tag{10}$$

Because the real part of the eigenvalues of A are negative, the state q_2 is asymptotically stable in the sense of Lyapunov. Therefore, q_2 always approaches zero. By this formal treatment of the state equations, an obvious fact is emphasized: the payload will always come to rest directly beneath the overhead support point. Therefore, precise positioning of the overhead support unit is equivalent to precise positioning of the payload. This fact enables the positioning module to be designed as a collocated controller of the overhead support unit instead of a non-collocated controller of the payload, thus simplifying the control objective significantly. This payload positioning strategy using a PD controller is illustrated in the block diagram of Fig. 14.

This module controls the position of the payload along the bridge axis. A desired position is issued to the

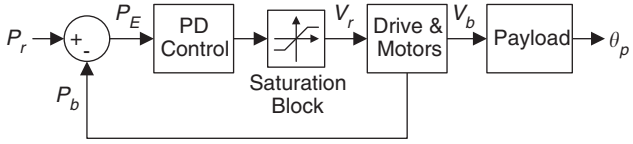

Fig. 14. Positioning control module.

controller as a position reference signal, P_r. On the MARC crane, a laser range sensor provides feedback of the bridge position, P_b. These two signals are compared to generate an error signal, P_E, which is sent to the PD block. In response to the error signal, the PD block generates a signal representing a desired bridge velocity. To prevent this signal from over-driving the bridge beyond a safe speed, a saturator has been inserted after the PD control block. The truncated reference velocity, V_r, is sent to bridge drive and motors, which causes the bridge to respond with velocity V_b. Finally, the payload responds to the bridge velocity with cable angle, θ_p.

The stability of the module may be determined by first considering the outputs, V_b and θ_p. The system is considered to be BIBO stable if for any bounded inputs into the system, the outputs, V_b and θ_p are also bounded. Secondly, because of the presence of hard nonlinearities (e.g. the saturation block, switching element, and rate limiter) one must also be concerned about the existence of limit cycles.

The BIBO stability of the system is quickly ascertained by considering the eigenvalues of H (the second-order plant in the drive and motors model), and the payload. For each, the eigenvalues have negative real parts. Therefore, for any bounded input into each of these plants, the outputs V_b and θ_p will also be bounded. The boundedness of V_b is immediately apparent because of the saturated boundedness of V_r. Given that V_b is bounded, θ_p is also bounded.

Predicting the presence of limits cycles in systems with "hard" nonlinearities, like saturation or rate limiting elements, has been performed for many years through the use of methods based on the sinusoidal input describing function. The describing function method is an approximating technique that allows one to predict a range of controller gains for which a system will likely not exhibit limit cycles. Because of the approximate nature of the technique, three kinds of inaccuracies are possible (Slotine & Li, 1991):

(1) The amplitude and frequency of the predicted limit cycle are not accurate.
(2) A predicted limit cycle does not actually exist.
(3) An existing limit cycle is not predicted.

Historically, the describing function method has been used on systems with exactly one nonlinear element. Recently, new studies have been conducted to better understand limit cycles that may exist due to multiple nonlinear elements (Anderson, 1998). For a system with

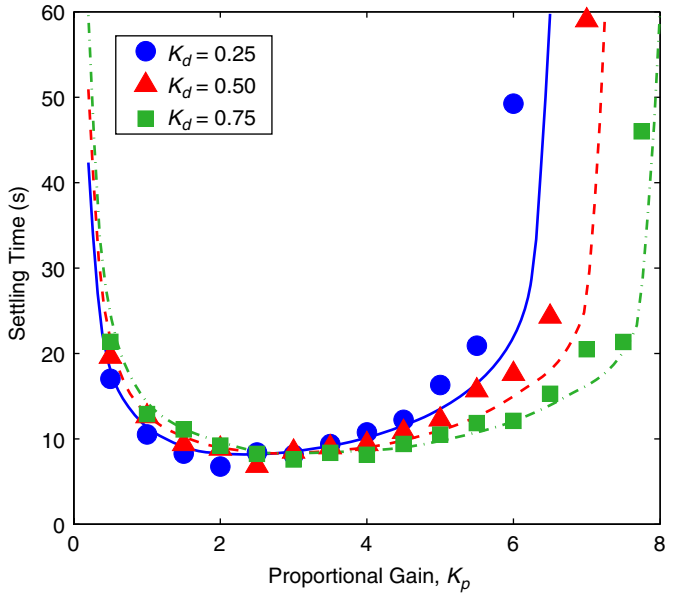

Fig. 15. Simulated and experimental settling times for the positioning module.

simultaneous rate limiting and saturation blocks in the loop, Amato et al. showed that the response of the nonlinear elements to a sustained sinusoidal input may be divided into 12 distinct classes, each of which has it's own unique describing function (Amato, Iervolino, Pandit, Scala, & Verde, 2000). Ten of the 12 describing functions are dependent on both the amplitude of the limit cycle, as well as the frequency. Therefore, to conduct a describing function analysis of the system in Fig. 14, one would have the challenging task of conducting 12 separate analysis, 10 of which are made more difficult because of the dependence on the limit cycle amplitude. The addition of the switching element compounds the difficulty.

In light of the fact that a successful describing function analysis of the system would yield approximate results at best, in addition to the fact that such an analysis would prove to be tedious and lengthy, a more straightforward approach to obtaining a range of acceptable controller gains is through simulations and experimental verification.

The bridge response to a commanded change in position of 2 m was repeatedly simulated as the proportional gain, K_p, and derivative gain, K_d, were systematically varied. To determine whether a particular gain combination sustained a limit cycle, the settling time of the bridge response was recorded for each trial. The settling times for different gain combinations are shown in Fig. 15 where the vertical axis represents the settling time[1] of the bridge and the horizontal axis represents the proportional gain used during the test. The solid, dashed, and dash-dotted lines in the figure represent the simulated bridge responses corresponding to derivative gains of 0.25, 0.50, and 0.75, respectively. Experimental results are overlaid with the simulation results and are represented as circles, triangles, and squares.

The characteristic of a sustained limit cycle is an infinite settling time, as seen on the right-hand side of the plot when the proportional gain is large. One should note that the infinite settling times on the left-hand side of the plot do not indicate limit cycles, but rather that the crane was under-actuated (i.e. the actuator gains were too low to move the crane).

The most important aspects of these results are that a close correlation between the predicted and actual settling times is revealed, and that the non-existence of limit cycles for a large range of gain combinations is verified. The gain combinations that prevented limit cycles in the tested 2-m crane movements will also prevent limit cycles for any arbitrary move distance. This is because limit cycles are only induced around the equilibrium vicinity of the commanded bridge position, and not in the transient positions of the crane. It is also important to note that the significant robustness of the module to limit cycles verified by these results is independent of the crane's cable length. This is because the payload responds to the position control module in a purely open-loop manner.

The positioning capabilities of the module are demonstrated in the experimental results of Fig. 16 where the bridge was commanded to move from the 0-m location to the 2-m location. The bridge response to the command is shown with the solid line. At the end of the commanded motion, the error between the desired position and the actual position of the bridge was 4 mm. However, because the module has no mechanism, such as an input shaper, to control the open-loop response of the payload, the payload is seen to oscillate about the desired position. This issue is

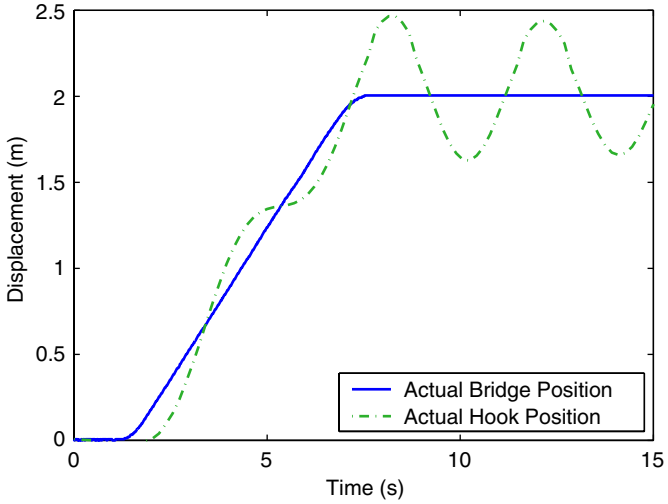

Fig. 16. Crane response to a position command of 2 m.

[1]Simulated settling times were obtained for numerous values of K_p while K_d was held constant at 0.25, 0.50, and 0.75. The solid lines in Fig. 15 represent best-fit curves passing through the data obtained during the simulated trails.

resolved in Section 4 where the input shaping and positioning modules are combined.

3.3. Disturbance rejection module

A control module was designed to eliminate the cable sway caused by external disturbances acting on the payload, such as wind. This type of disturbance may be modeled as inducing a disruptive angle, θ_d, summed with the undisturbed angle, θ_p, to produce the actual cable angle of the system, θ_a.

The module designed to eliminate these types of disturbances along the bridge axis is schematically shown in Fig. 17. Disturbance rejection is accomplished by making use of a machine vision system to provide sensory feedback of the actual cable angle, θ_a. This information is utilized in a PD block to generate velocity commands that damp out the disruptive oscillations. These corrective velocity signals, V_c, are added to the original reference velocity signal, V_s. To maintain a maximum velocity limit, a saturation block truncates excessive velocities prior to being sent to the drives and motors.

A key element of the disturbance rejection module is the plant models that respond to velocity reference signals, V_s. The purpose of the models is to provide a means by which payload oscillations caused by external disturbances may be distinguished from payload oscillations caused by desired motion of the overhead support unit. If one assumes that V_s has maximum and minimum values within the thresholds of the saturation block, then in the absence of any disruptive angle, θ_d, the response of the model and the response of the actual system will be nearly equal. As a result, no corrective velocity signal will be generated. If, however, a disturbance is present, then the comparison of θ_m to θ_a will cause the PD control to generate the correcting command, V_c (a correcting command could also be generated in the absence of a disturbance if there are gross inaccuracies in modeling parameters or sensing errors).

Limit cycle and BIBO stability of the module were verified in the same manner discussed previously for the positioning module. For BIBO stability, the eigenvalues of the linear plants, and signal boundedness were considered. For the limit cycle analysis, a process of simulation and experimental verification confirmed that a substantial range of controller gains exist for which limit cycles do not occur. This range of controller gains was verified for cable lengths between 2.5 and 6 m. The verification process revealed that an effective combination of proportional and derivative controller gains over this range of cable lengths was $K_p = 2$ and $K_d = 2$.

The disturbance rejection capabilities are demonstrated in Fig. 18, where the bridge position is shown with a solid line and the payload position is overlaid with a dashed line. Here, a disturbance acted on the payload causing an oscillatory response. The disturbance rejection module was activated at approximately time $t = 7$ s. The oscillations of the payload were mostly damped out by time $t = 15$ s, a time duration of approximately two oscillation periods.

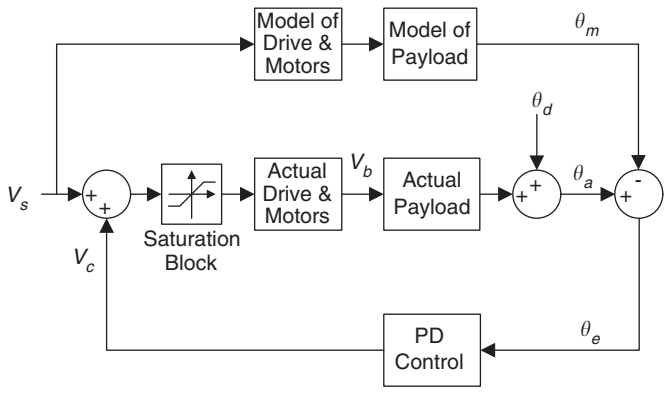

Fig. 17. Disturbance rejection control module.

4. Combining the three control modules

This section presents an architecture in which the three individual control modules are combined into one complete control scheme. In doing so, the combined controller possesses the collective attributes of the individual controllers, namely, suppression of motion-induced oscillations, precision positioning capabilities, and the capacity to reject disturbance-induced oscillations. As a first step in describing how the three modules may be combined, Section 4.1 first combines the input shaping module with the positioning module. Later, Section 4.2 adds the disturbance rejection module.

4.1. Combining input shaping and positioning modules

The positioning module of Section 3.2 generates a reference velocity, V_r, which drives the bridge toward a desired set point. This signal, though enabling the crane to achieve a desired position, also induces oscillations in the payload. A more desirable control scheme allows precise positioning of the crane, while also eliminating these motion-induced oscillations. To this end, the input shaping module of Section 3.1 can be incorporated with the positioning module. The combined control scheme is shown in Fig. 19.

In this combined scheme, the PD and saturating blocks still generate a signal, V_r, which drives the crane toward a desired position; however, this signal is now modified by the input shaping module to produce a shaped signal, V_s. In this way, the shaped signal serves the dual purpose of driving the crane toward a desired position, while also preventing motion-induced oscillations of the payload.

With the insertion of the input shaper into the forward path of the positioning control loop, the question of system stability arises. This is because the input shaper effectively delays a portion of the signal by a time equal to the

duration of the shaper. In Section 3.2 two analysis tools were used to determine the stability of the positioning module, namely, the BIBO stability analysis, and a simulation/experimentation technique that determined the existence of limit cycles. These tools were again used to verify that the shaper-in-the-loop system is BIBO stable, and that a large range of controller gains exists that prevent limit cycles. In addition, a third analysis tool was used to gain a deeper understanding of the shaper-in-the-loop system; the combined control was considered from the perspective of the Laplace domain (Huey & Singhose, 2005).

A simplified block diagram of the combined control can be obtained by neglecting the three hard nonlinearities, namely, the saturation block, and the nonlinear switch and rate limiter within the drive and motors block. These eliminations yield the entirely linear closed-loop system shown in Fig. 20.

Here, $C(s)$, $I_{ZV}(s)$, and $G(s)$ are the Laplace representations of the PD control block, a ZV input shaper, and the drive and motors block, respectively.

For $C(s)$, we have

$$C(s) = K_o(K_p + K_d s), \tag{11}$$

where K_p and K_d are the proportional and derivative gains, respectively, and K_o is an open-loop scaling factor.

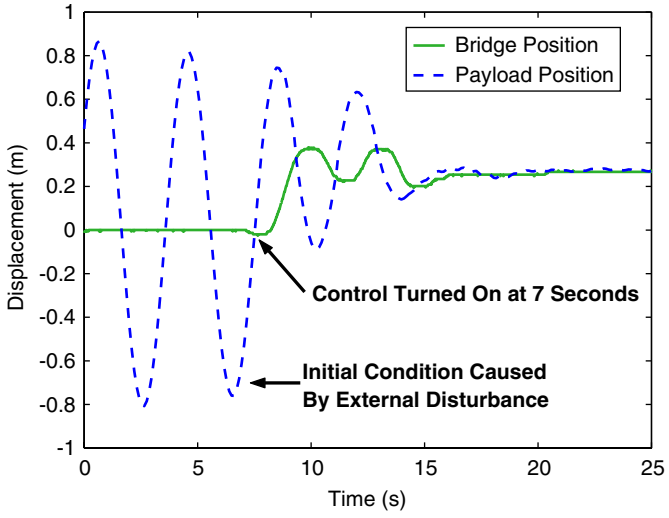

Fig. 18. Cancellation of disturbance-induced oscillations.

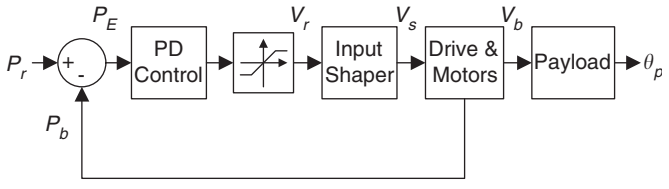

Fig. 19. Combined input shaping and positioning controller.

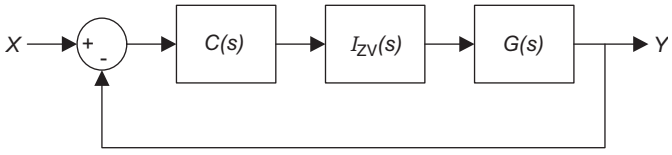

Fig. 20. Simplified shaper-in-the-loop system.

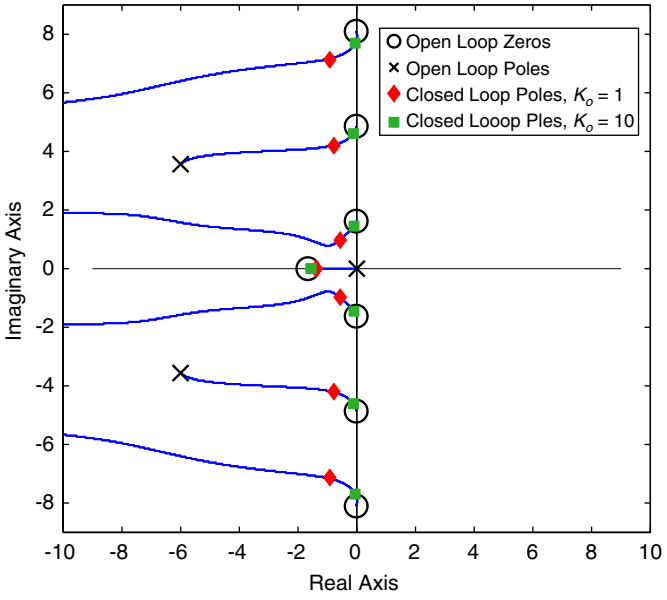

Fig. 21. Root locus plot of linearized system.

For $G(s)$, we have

$$G(s) = \frac{\omega_H^2}{s(s^2 + 2\zeta\omega_H s + \omega_H^2)}, \tag{12}$$

where ω_H and ζ are the natural frequency and damping ratio associated with the heavily damped system within the drive and motors model.

Recognizing that a ZV input shaper is constituted by an impulse of magnitude A_1, followed by an impulse of magnitude A_2, delayed by time t_2, one may represent the shaper in the Laplace domain as

$$I_{ZV}(s) = A_1 + A_2 e^{-st_2}. \tag{13}$$

Given the Laplace representation of each element, a root-locus of the system may be obtained. Assigning the values of 0.8 and 0.5 to the proportional and derivative gains, respectively, one obtains the root-locus shown in Fig. 21.

The open-loop poles, shown with the black X's, are contributed by the transfer function, $G(s)$. The input shaper contributes an infinite column of open-loop zeros along the imaginary axis, shown with the black circles. And finally, $C(s)$ contributes a single open-loop zero with negative real part, also shown with a black circle. The closed-loop poles of the system are represented by diamonds when the scaling

gain is set to 1.0. The closed-loop poles of the system are represented by squares when the scaling gain is set to 10.0.

The significant feature of this root-locus is that the poles of the closed-loop system remain strictly in the negative left-hand plane for the range of scaling gains shown. Therefore, for the linearized system of Fig. 20, one is assured of stability.

The Laplace domain analysis does not guarantee the stability of the nonlinear system in Fig. 19. It does, however, serve to provide insight into the dynamics of shaper-in-the-loop systems in general. It also gives one an understanding of how the system in Fig. 19 performs when operating in its linear region.

The positioning and oscillation reducing properties of the combined positioning and shaping control were verified experimentally on the MARC crane. The crane was driven to 25 arbitrary reference positions while coordinate information about the bridge and payload were gathered. Both the residual oscillation amplitude of the payload and the final positioning error were recorded for each of the 25 trials. The response of the crane to a typical position command is shown in Fig. 22. For this experiment, the crane started at the 0-m location and was then commanded to move to the 2-m location. The solid curve represents the actual position of the bridge throughout the experiment; the dashed curve represents the position of the payload.

This plot contrasts sharply with Fig. 16 where an identical position command was issued to the positioning module without input shaping. The contrast between these two figures demonstrates the effectiveness of the combined input shaping and positioning controller at precise positioning and minimizing motion-induced payload oscillations.

The positioning error result for each of the 25 trials is shown in Fig. 23, while the residual oscillation amplitude of the payload for each of the 25 trials is shown in Fig. 24. The vertical axis in Fig. 23 represents the final positioning error between the desired bridge position and the actual bridge position. The vertical axis of Fig. 24 represents the residual peak-to-peak oscillation amplitude of the payload. Notice that this axis has been normalized to the residual peak-to-peak oscillation amplitude for unshaped crane motion.

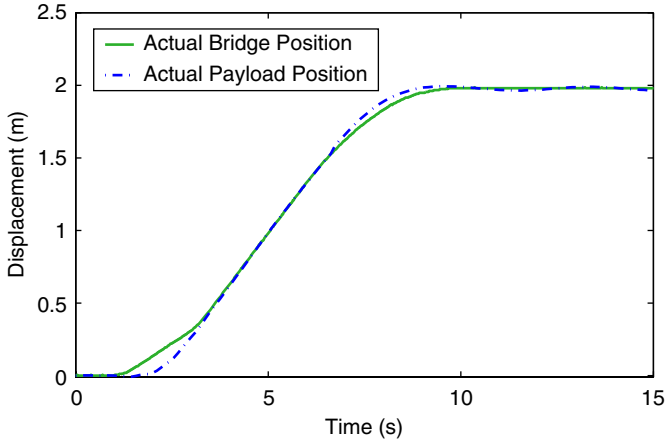

Fig. 22. Crane response to a position command of 2 m using the shaper-in-the-loop control system.

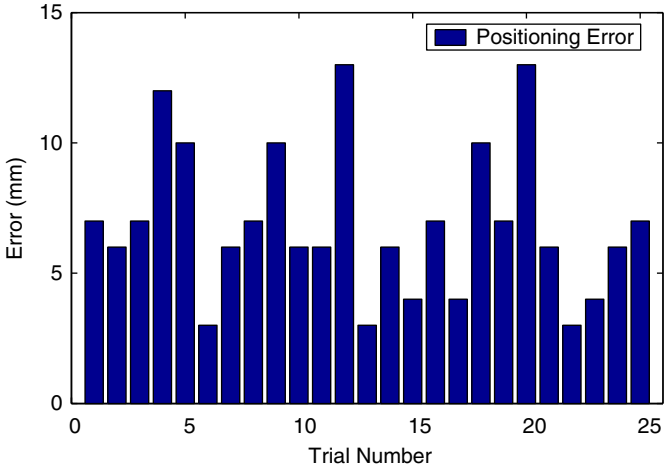

Fig. 23. Final positioning error of the crane.

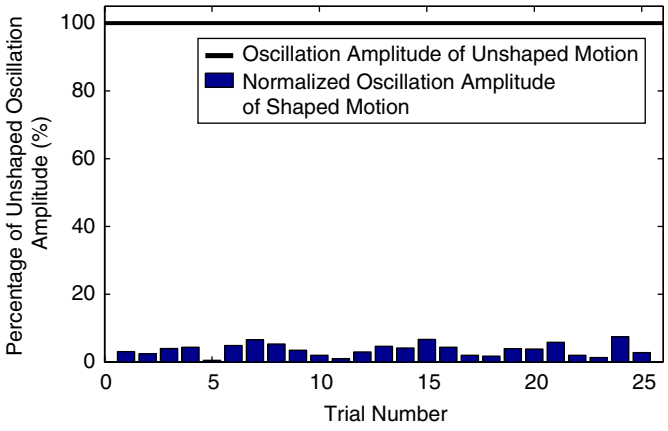

Fig. 24. Residual payload oscillation amplitude of the crane.

These figures demonstrate that with the implemented control, the crane may be reliably positioned to within approximately 1 cm of a commanded position while keeping the oscillations to approximately 5% of the oscillation amplitude normally excited with unshaped motion.

4.2. Combining input shaping, positioning, and disturbance rejection modules

The disturbance rejection controller from Section 3.3 monitors the cable angle of the payload while the crane follows an arbitrary reference velocity. If the reference velocity issued to the module is within the thresholds of the saturation block, then the control can distinguish between motion and disturbance-induced payload oscillations.

A suitable reference velocity for the disturbance module is the shaped reference velocity generated by the combined input shaping and positioning controller. By design, this signal is already bounded between the upper and lower

thresholds of the saturation block. Furthermore, it has been shaped to cancel motion-induced oscillations in the payload. To use this signal as the input to the disturbance controller, the disturbance controller may be combined with the input shaping and positioning controller in the manner previously shown in Fig. 7.

Referring back to Fig. 7, the input shaping and positioning control generates a shaped reference velocity that is used as an input to the disturbance rejection module. The module receives the shaped signal, V_s, and tracks it, while also rejecting disturbances. Because V_s continually drives the crane toward a desired set point, the disturbance rejection module will achieve the dual objectives of positioning and disturbance rejection. Furthermore, because V_s is an input-shaped command, motion-induced oscillations of the payload will be reduced. In this way, the combined input shaping, positioning, and disturbance rejection controller eliminates motion-induced oscillations, rejects disturbances, and enables precise positioning of the payload.

The control system was implemented and rigorously tested on the MARC crane. One method of evaluating the three attributes of the control involved commanding the crane to move to a desired location. After coming to rest at the desired position, an external disturbance was introduced. Typical performance of the controller, in response to this experiment, is demonstrated in Fig. 25a. Here the crane was commanded to move to the 4-m location. One may observe that the shaped velocity signals of the positioning controller prevented motion-induced oscillations of the payload, while also driving the crane precisely to the 4-m location. Later, when the external disturbance was introduced, the control system eliminated the disruptive oscillations while returning the payload to the desired position.

Another experiment was conducted in which the crane was commanded to move 4 m. While in transit, an external disturbance was applied to the payload. The results of this experiment are shown in Fig. 25b. Again the control system prevented motion-induced oscillations, rejected disturbances, and precisely positioned the payload.

The BIBO stability of the control system is assured based on the previous analyses of each of the individual modules. Predicting the existence of limit cycles for the combined control was accomplished by using the simulation/experimental verification method used for the position and disturbance rejection modules. It was confirmed that the control does not exhibit limit cycles given a suitable combination of controller gains. This was verified over a range of cable lengths varying from 2.5 to 6 m. Fig. 26 demonstrates the non-existence of limit cycles over this range for one specific combination of gains. The data shown represents the settling time[2] of the bridge in

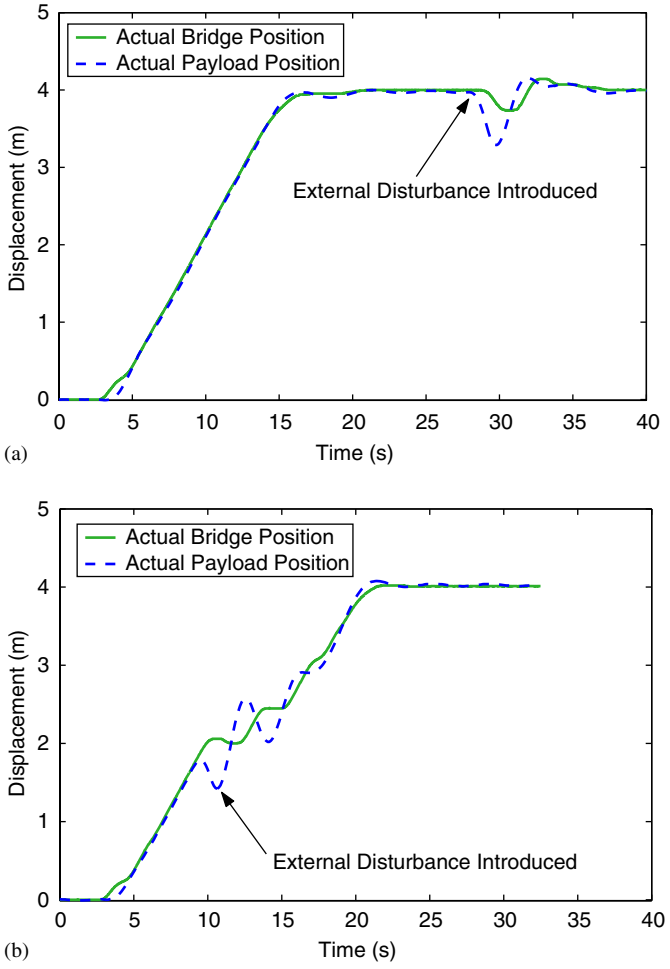

Fig. 25. Bridge and payload response using the combined control system: (a) disturbance introduced after crane reached final position and (b) disturbance introduced in transit.

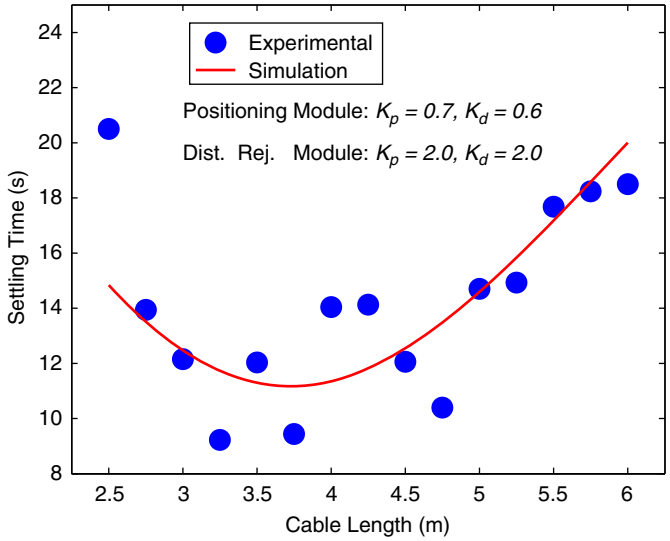

Fig. 26. Simulated and experimental settling times for the combined control.

[2]Simulated settling times were obtained for the 15 different cable lengths experimentally tested. The solid line in Fig. 26 represent best-fit curve passing through the data obtained during the simulated trails.

response to disturbances introduced into the payload. At each cable length tested, the crane hook was initially disturbed from a desired location such that the initial swing amplitude was 16° from vertical. The control system eliminated the disturbances, while restoring the hook to the desired positions. It should be noted that although one combination of controller gains has been used to eliminate disturbances over this range of cable lengths, more favorable gain combinations may be chosen at each cable length to further reduce settling time.

The cumulative experimental results validate the ability of the control system to achieve the three objectives of precise positioning, elimination of motion-induced payload oscillations, and disturbance rejection over a large range of cable lengths.

5. Conclusion

A control scheme was developed to enable precise positioning of a crane payload, while motion and disturbance-induced oscillations are eliminated. The combined input shaping, positioning, and disturbance rejection controller takes into account the special properties of cranes: the predominantly single-mode nature of the payload dynamics, the known frequency range of the dominant mode, and the nonlinear effects of common actuating AC induction motors and vector drives. The control scheme utilizes a unique architecture that allocates individual control objectives to modules most suited for the task. Feedback control is used for positioning and disturbance rejection, and input shaping is used for motion-induced sway reduction. Several methods for determining stability were discussed and evaluated. The controller was implemented and tested on a 10-ton bridge crane at Georgia Tech. Experimental results verified that the control system can significantly reduce motion and disturbance-induced cable sway, while enabling precise payload positioning.

Acknowledgements

This project would not have been possible without the generous support of CAMotion and Siemens. They provided the technical support and physical hardware necessary for this research.

References

Amato, F., Iervolino, R., Pandit, M., Scala, S., & Verde, L. (2000). Analysis of pilot-in-the-loop oscillations due to position and rate saturations. In *Proceedings of the conference on decision and control*, Sydney, Australia.

Anderson, M. R. (1998). Pilot-induced oscillations involving multiple nonlinearities. *Journal of Guidance, Control, and Dynamics*, *21*.

Fang, Y., Dixon, W. E., Dawson, D. M., & Zergeroglu, E. (2001). Nonlinear coupling control laws for a 3-DOF overhead crane system. In *Proceedings of the 40th IEEE conference of decision and control*, Orlando, FL, USA.

Fliess, M. (1989). Automatique et Corps Differentiels. *Forum Mathematicum*, *1*, 227–238.

Fliess, M., Levine, J., & Rouchon, P. (1991). A simplified approach of crane control via a generalized state-space model. In *Proceedings of the 30th conference on decision and control*, Brighton, England.

Gustafsson, T., & Heidenback, C. (2002). Automatic control of unmanned cranes at the Pasir Panjang terminal. In *Proceedings of the 2002 IEEE international conference on control applications*, Glasgow, Scotland, UK.

Huey, J. R., & Singhose, W. (2005). Stability analysis of closed-loop input shaping control. In *Proceedings of the 16th IFAC world congress*, Prague.

Kenison, M., & Singhose, W. (1999). Input shaper design for double-pendulum planar gantry cranes. In *Proceedings of the IEEE conference on control applications*, Hawaii.

Khalid, A., Singhose, W., Huey, J., & Lawrence, J. (2004). Study of operator behavior, learning, and performance using an input-shaped bridge crane. In *Proceedings of the conference on control applications*, Taipei, Taiwan.

Kim, Y.-S., Hong, K.-S., & Sul, S.-K. (2004). Anti-sway control of container cranes: Inclinometer, observer, and state feedback. *International Journal of Control, Automation, and Systems*, *2*, 435–449.

Lewis, D., Parker, G. G., Driessen, B., & Robinett, R. D. (1998). Command shaping control of an operator-in-the-loop boom crane. In *Proceedings of the American Control Conference*, Philadelphia, PA.

Moustafa, K. A. F. (2001). Reference trajectory tracking of overhead cranes. *Journal of Dynamic Systems, Measurement, and Control*, *123*, 139–141.

O'Connor, W. J. (2003). A gantry crane problem solved. *Journal of Dynamic Systems, Measurement, and Control*, *125*, 569–576.

Piazzi, A., & Visioli, A. (2002). Optimal dynamic-inversion-based control of an overhead crane. *IEE Proceedings-Control Theory and Applications*, *149*, 405–411.

Singer, N., Singhose, W., & Kriikku, E. (1997). An input shaping controller enabling cranes to move without sway. In *Proceedings of the ANS seventh topical meeting on robotics and remote systems*, Augusta, GA.

Singer, N. C., & Seering, W. P. (1990). Preshaping command inputs to reduce system vibration. *Journal of Dynamic Systems, Measurement, and Control*, *112*, 76–82.

Singhose, W., Porter, L., Kenison, M., & Kriikku, E. (2000). Effects of hoisting on the input shaping control of gantry cranes. *Control Engineering Practice*, *8*, 1159–1165.

Slotine, J.-J. E., & Li, W. (1991). *Applied nonlinear control*. Englwood Cliffs, NJ: Prentice-Hall, Inc.

Smith, O. J. M. (1957). Posicast control of damped oscillatory systems. *Proceedings of the IRE*, *45*, 1249–1255.

Sorensen, K. L. (2005). *A combined feedback and command shaping controller for improving positioning and reducing cable sway in cranes*. Master's thesis, Department of Mechanical Engineering, Georgia Institute of Technology, Atlanta.

Sorensen, K. L., Singhose, W., & Dickerson, S. (2005). A controller enabling precise positioning and sway reduction in cranes with on–off actuation. In *Proceedings of the 16th international federation of automatic control world congress*, Prague.